

# Vesicle Formation from Temperature Jumps in a Nonionic Surfactant System

Karin Bryskhe,\* Sanja Bulut, and Ulf Olsson

Physical Chemistry 1, Center for Chemistry and Chemical Engineering, Lund University, P.O. Box 124, S-221 00 Lund, Sweden

Received: October 18, 2004; In Final Form: December 22, 2004

When heating a dilute sample of the binary system of tetraethyleneglycol dodecyl ether ( $C_{12}E_4$ ) and water from the micellar phase ( $L_1$ ) into the two-phase region of a lamellar phase ( $L_\alpha$ ), and excess water (W) vesicles are formed. During heating, one passes a region of phase separation in the micellar phase ( $L_1' + L_1''$ ) where the initial micelles rapidly fuse into larger aggregates forming the concentrated  $L_1$  phase ( $L_1''$ ) with a structure of branched cylindrical micelles, a so-called “living network”. The static correlation length of the micelles are increasing with increasing concentration, from ca. 10 nm to 80 nm in the concentration range of 0.0001 g/cm<sup>3</sup>–0.0035 g/cm<sup>3</sup>. The overlap concentration was determined to 0.0035 g/cm<sup>3</sup>. When the temperature reaches the  $L_1' + L_\alpha$  region the network particles transform into bilayer vesicles with a z-average apparent hydrodynamic radius in the order of 200 nm depending on the composition. The size of the final vesicles depends on the extent of aggregation/fusion in the  $L_1' + L_1''$  region and hence on the rate of heating. The aggregation/fusion in the  $L_1' + L_1''$  is slower than diffusion-limited aggregation, and it is shown that 1/100 of the collisions are sticky results in the fusion event.

## 1. Introduction

One class of water-soluble surfactants are the alkyl oligo-(ethylene oxide) surfactants often abbreviated as  $C_nE_m$ . These surfactants exist in a wide range of different compositions and display a rich phase behavior in water, depending on parameters such as surfactant chemical structure, temperature, concentration, and additives.<sup>1–5</sup> The  $C_nE_m$  surfactants have been investigated for different applications for pharmaceutical use, as a component in different drug delivery systems, in formulations of cosmetics, and as detergents.<sup>6,7</sup> In this work we study the  $C_{12}E_4$ /water system, which is known to form vesicles at low concentrations.<sup>8–10</sup> The  $C_nE_m$  surfactant systems are useful model systems because the spontaneous curvature,  $H_0$ , can be conveniently tuned by varying the temperature.<sup>11,12</sup> At lower temperatures the surfactant film prefers to curve away from water ( $H_0 > 0$ ), and an aqueous micellar solution is stable. Spherical micelles are formed when  $H_0 = 1/l_s$  or higher. With decreasing  $H_0$ , there is first the formation of cylindrical micelles forming a so-called “living polymer” system.<sup>13</sup> Upon a further decrease of  $H_0$ , branches between micelles are formed, and the system turns into a “living network” system.<sup>14</sup> Branch points are regions of lower curvature, and in the network structure, the average mean curvature depends on the density of branch points, which in turn is coupled to the surfactant concentration. The higher the concentration, the higher is the maximum branching density. At lower values of  $H_0$  the network therefore has a finite swelling, and the system undergoes a liquid–liquid-phase separation. In nonionic surfactants, this liquid–liquid-phase separation is a general feature and is often referred to as “clouding” because of the appearance of the phase separation. In many  $C_nE_m$ –water systems the liquid–liquid-phase separation can be understood in terms of the finite swelling of “living networks”.<sup>15</sup> Exceptions are for example surfactants with very long ethylene oxide (EO) chains

where the direct water–EO interaction appears to be responsible for the phase separation, and where the phase separation temperature is very high, similar to the phase separation temperature of the homopolymer, PEO. At higher temperatures, on the other hand, the film prefers curvature toward water ( $H_0 < 0$ ). When  $H_0$  is weakly negative, a sponge phase is stable,<sup>16</sup> while the lamellar phase has maximum stability when  $H_0 \approx 0$ . The temperature at which  $H_0 = 0$  we denote  $T_0$ . Aqueous vesicles mainly form when  $H_0$  is weakly positive.

Vesicles are bilayer shells enclosing a pool of solvent.<sup>17–21</sup> They are generally metastable structures where thermodynamic equilibrium corresponds to a lamellar phase, possibly coexisting with excess solvent. However, there are also several reports in the literature claiming thermodynamically stability.<sup>22–25</sup> The problem of thermodynamic equilibrium can be a difficult issue to reveal experimentally. The coarsening mechanism of Ostwald ripening is expected to be very slow in vesicle systems and may even lead to a kinetically trapped size distribution.<sup>26</sup> Hence, if vesicle fusion is rare a vesicle preparation may remain stationary for long periods of time.

Vesicles are often prepared by dispersing a lamellar phase by e.g. extrusion or sonication.<sup>27</sup> In mixed systems vesicles may also form upon a rapid dilution of a mixed micellar solution,<sup>28</sup> where a highly soluble component is extracted from the surfactant mixture upon dilution leaving a surfactant composition having a spontaneous curvature near zero. The mechanism of vesicle formation in this dilution quench method has been characterized and analyzed in detail recently and involves micellar growth into bilayer disks that eventually close into vesicles.<sup>29–31</sup> In recent publications,<sup>32,33</sup> we reported vesicle formation in dilute aqueous solutions of the bilayer forming PEO–PPO–PEO block copolymer L121 by simply heating samples from a homogeneous liquid phase into a two-phase region where a concentrated lamellar phase coexists with an excess dilute block copolymer solution. The spontaneous curvature of PEO–PPO–PEO block copolymers has similar

\* Corresponding author phone: +46 46 222 82 04; fax: +46 46 222 44 13; e-mail: Karin.Bryskhe@fekem1.lu.se.



ments including a solid-state, diode-pumped Nd:YAG laser from Coherent operating at 532 nm and at a constant output power of 400 mW, which is variable with an external attenuator from Newport Corp., USA. For DLS measurements, two multiple delay time digital correlators (ALV-5000/E and ALV-5000/FAST) with a total of 320 exponentially spaced channels were employed to construct the normalized time-correlation function of the scattered intensity,  $C(q, t)$ , which can be written as<sup>36</sup>

$$C(q, t) = aB[\int_0^\infty d\Gamma G(\Gamma)e^{-\Gamma t}]^2 + B \quad (2)$$

if we neglect the random noise contribution. Here,  $a$  and  $B$  are constants and  $G(\Gamma)$  is the intensity weighted relaxation frequency distribution function, where  $\Gamma$  is the inverse of the relaxation time,  $\tau$ .  $G(\Gamma)$  was constructed from the experimental  $C(q, t)$  using the inverse Laplace transform routine provided by the ALV software.  $\Gamma$  is related to a collective diffusion coefficient,  $D$ , through  $\Gamma = Dq^2$ , where  $q = (4\pi n/\lambda_0)\sin(\theta/2)$  is the magnitude of the scattering vector. Here,  $n$  is the refractive index of the solution,  $\lambda_0$  is the wavelength in a vacuum, and  $\theta$  is the scattering angle. At low concentrations,  $D \approx D_0$ , where  $D_0$  denotes the free diffusion coefficient related to the hydrodynamic radius,  $R_H$ , according to the Stokes–Einstein relation

$$R_H = \frac{k_B T}{6\pi\eta_0 D_0} \quad (3)$$

Here  $k_B$  is the Boltzmann constant,  $T$  is the absolute temperature, and  $\eta_0$  is the viscosity of the solvent. The SLS measurements were performed on surfactant aqueous solutions (0.01–5 wt %). Subtraction of the scattering from the solvent water and from the background was also done. Toluene was used as a reference standard. The intensities were converted into absolute scattering intensities  $\Delta R(\theta)$  (i.e., “excess Rayleigh ratios”). The excess Rayleigh ratio of the sample was calculated from<sup>36</sup>

$$\Delta R(\theta) = \frac{\langle I(\theta) \rangle}{\langle I_{ref}(\theta) \rangle} R_{ref}(\theta) \left( \frac{n}{n_{ref}} \right)^2 \quad (4)$$

where  $\langle I(\theta) \rangle$  and  $\langle I_{ref}(\theta) \rangle$  are the average excess scattering intensity of the solution and the average scattering intensity of the reference solvent toluene,  $R_{ref}(\theta) = 26.0 \times 10^{-4} \text{ m}^{-1}$  is the Rayleigh ratio of toluene, and  $n$  and  $n_{ref}$  are the index of refraction of the solution and the reference solvent, respectively.<sup>37</sup> The apparent micellar molecular weight was determined experimentally by plotting  $Kc/\Delta R(q)$  versus  $q^2$ , where  $K = 4\pi^2 n^2 (dn/dc)^2 / (N_A \lambda_0^4)$  and extrapolating to  $q = 0$ .

### 3. Micelle Size in the L<sub>1</sub> Phase

To determine the size of the initial micelles involved in the temperature jumps, we have performed static and dynamic light scattering experiments in the L<sub>1</sub> phase. The concentration range investigated was 0.01–5 wt % C<sub>12</sub>E<sub>4</sub>, and the experiments were performed at 2 °C and 5 °C. C<sub>12</sub>E<sub>4</sub> is known to form large nonspherical micelles in the L<sub>1</sub> phase.<sup>38</sup> This is also seen from the strong  $q$ -dependence of the scattered intensity as illustrated in Figure 2 where we show the scattering curves of some selected concentrations below the overlap concentration.

The scattered intensity shows a Lorentzian  $q$ -dependence, and from the scattering curves we can determine the apparent molecular mass  $M_{app}$  and the static correlation length  $\xi_s$  from

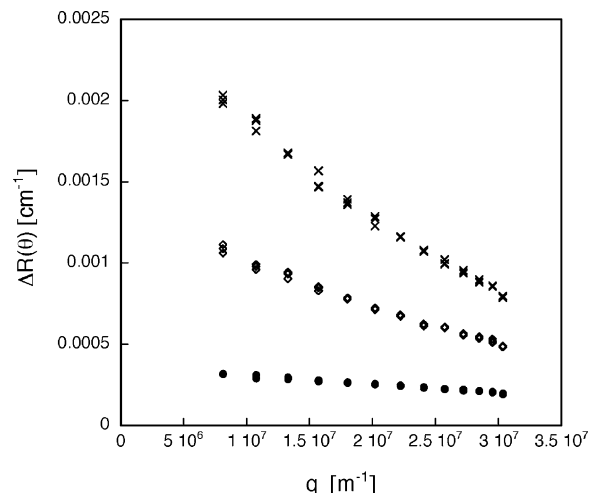


**Figure 2.** Excess Rayleigh ratio as a function of the scattering vector at 5 °C for C<sub>12</sub>E<sub>4</sub> in aqueous solution for some selected concentrations: (●) = 0.07 wt %, (◇) = 0.15 wt %, (×) = 0.25 wt %.

plotting the inverse of the absolute scattered intensity versus  $q^2$ , according to<sup>36</sup>

$$\frac{K(c-\text{CMC})}{\Delta R(\theta)} = \frac{1}{M_{app}} (1 + q^2 \xi_s^2) \quad (5)$$

where CMC is the critical micelle concentration, which is approximately 0.003 wt %.<sup>1</sup> The obtained values of  $\xi_s$  and  $M_{app}$  are presented as a function of the surfactant concentration in Figure 3 a and b, respectively.

On the low concentration side, the rapid increase in micellar size with increasing concentrations is clearly observed. The overlap concentration,  $c^*$ , can be determined to 0.35 wt % from the maxima in Figure 3a,b.

Above  $c^*$ ,  $\xi_s$  does no longer report on the micellar size but is now related to the mesh size of the entangled wormlike micelles forming a transient network which decreases with increasing concentration. Also the apparent molar mass decreases at higher concentrations as interactions lead to a decrease of the osmotic compressibility. In fact, the molar mass appearing in eq 5 is only an apparent value since it is influenced by intermicellar interactions.

In an attempt to include intermicellar interactions in the analysis of light scattering data from wormlike micellar systems, Schurtenberger et al.<sup>39</sup> turned to a renormalization group theory originally developed for semidilute polymer solutions, modifying it to allow for a concentration dependent molecular weight distribution. Schurtenberger et al. have analyzed some different systems,<sup>40,41</sup> including the water–C<sub>16</sub>E<sub>6</sub> system,<sup>42</sup> which is closely related to ours. A general result from their analysis is that the micellar molecular weight, if assumed to obey the power law  $M_w = B_1 c^\gamma$ , show a significantly stronger concentration dependence than what is predicted by classical mean field models. While mean field models predict values of 0.5–0.6 for the exponent  $\gamma$ , Schurtenberger et al. obtained  $\gamma = 1.1$ <sup>42</sup> or 1.2.<sup>39</sup> The reason for this discrepancy is at present not understood.

Following the approach of Schurtenberger we have analyzed also the present data set in terms of the modified renormalization group theory. Here, the static structure factor  $S(0)$  is expressed as a function of the reduced concentration  $X$ <sup>43</sup>

$$M_{app} = M_w S(0) = M_w f(X) \quad (6)$$

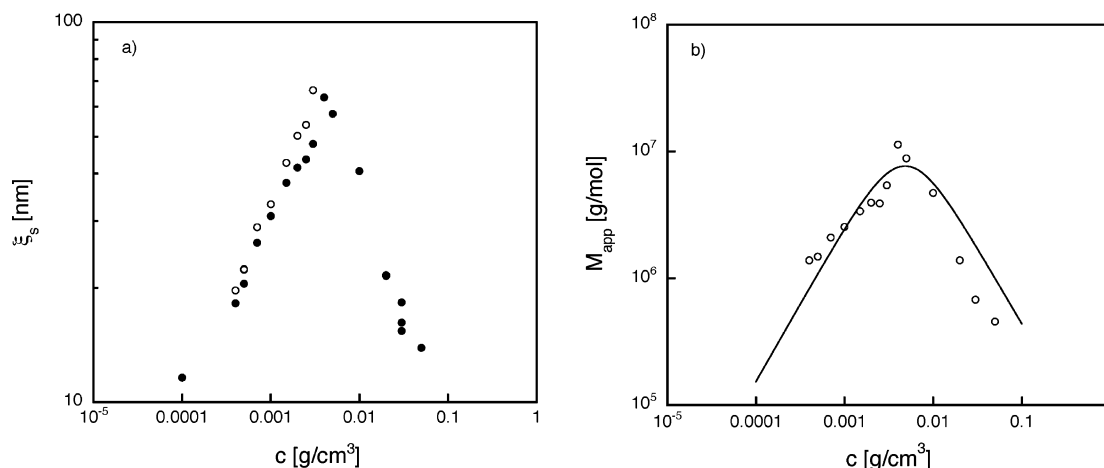


**Figure 3.** (a) Static correlation length  $\xi_s$  of C<sub>12</sub>E<sub>4</sub> in aqueous solution as a function of concentration at 5 °C (○) and 2 °C (●). The correlation length is increasing with concentration for both temperatures (indicating growth of wormlike micelles) until it reaches a maximum value, at the overlap concentration, when it begins to decrease due to scattering from mesh size rather than micelles. (b) Apparent molar mass  $M_{app}$  of C<sub>12</sub>E<sub>4</sub> in aqueous solution as a function of concentration at the temperature, 2 °C (○).

where the function  $f(X)^{-1}$  can be written as<sup>44</sup>

$$f(X)^{-1} = 1 + \frac{1}{8} \left( 9X - 2 + \frac{2 \ln(1 + X)}{X} \right) \exp \left( \frac{1}{4} \left[ \frac{1}{X} + \left( 1 - \frac{1}{X^2} \right) \ln(1 + X) \right] \right) = S(0)^{-1} \quad (7)$$

with  $X$  given by<sup>45,46</sup>

$$X = 2.10 B_1^{(3\nu-1)} B_2 c^{[\gamma(3\nu-1)+1]} \quad (8)$$

The two exponents,  $\gamma$  and  $\nu$ , arise from assuming  $M_w = B_1 c^\gamma$ , as mentioned above, and that radius of gyration  $R_g \propto M^\nu$ . A more detailed description of the model can be found in the work of Schurtenberger et al.<sup>39,42</sup>

A best fit of eqs 6–8 to the data in Figure 3b is shown as a solid line, where the exponent,  $\nu = 0.588$ , was kept constant. The obtained values of the parameters were  $\gamma = 1.2$ ,  $B_1 = 1.21 \times 10^{10}$ , and  $B_2 = 2.78 \times 10^{-4}$ , respectively, all of which are very close to the values obtained in the related water–C<sub>16</sub>E<sub>6</sub> system.<sup>42</sup>

As mentioned above, the reason for the large growth exponent is not understood. We note that the present system, in common with the C<sub>16</sub>E<sub>6</sub><sup>47</sup> and the water–lecithin–isooctane<sup>14</sup> systems, forms a “living network” at higher concentration. In the present system, solutions at higher concentrations are not even visually viscoelastic. The fact that the system forms branches should influence the growth law, but to what extent has to our knowledge not yet been analyzed.

In the temperature jump experiments, which will be discussed below, only low concentrations,  $\leq 0.05$  wt %, were used. At the concentration 0.05 wt % and  $T = 5$  °C the value of  $M_{app}$  corresponds to an average aggregation number of approximately 470. The radius of gyration can at this low concentration be determined from the static correlation length according to  $R_g = \sqrt{3}\xi_s$ . At 0.05 wt %,  $R_g \approx 35$  nm. The micelles are much smaller than the vesicles formed after the temperature jumps.

#### 4. Temperature Jumps into the L<sub>1</sub>' + L<sub>α</sub> Region and Formation of Vesicles

After having analyzed the self-assembly in the L<sub>1</sub> phase we now turn to experiments where dilute samples, initially equi-

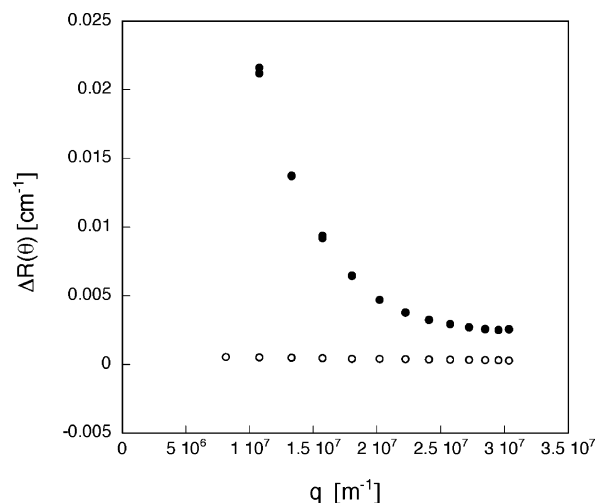


**Figure 4.** Excess Rayleigh ratio as a function of the scattering vector before and after the temperature jump. A sample of 0.1 wt % C<sub>12</sub>E<sub>4</sub> is measured at 2 °C (○) and 45 °C (●).

brated in the micellar phase, are suddenly brought to higher temperatures where lamellar structures are stable. These temperature jumps were performed from  $\approx 5$  °C, to the L<sub>1</sub>' + L<sub>α</sub> region at 35 °C or 45 °C, by rapidly (within  $\approx 3$  s) moving the sample from a 5 °C water bath to the cell house of the light scattering instrument, equilibrated at 35 °C or 45 °C. The temperature jump results in the formation of larger aggregates as illustrated in Figure 4 where we show the Rayleigh ratio as a function of the scattering vector as obtained by SLS experiment before and after a temperature jump. The Rayleigh ratio after the temperature jump to 45 °C is almost  $q^{-2}$  dependent which indicates a bilayer structure.<sup>48</sup> The size distribution after the temperature jump is stable for at least 43 h.

It has previously been shown that C<sub>12</sub>E<sub>4</sub> can form vesicles in this region of the phase diagram,<sup>8,9</sup> and in what follows we will assume that the large aggregates formed after the temperature jumps are, because of the low concentrations, unilamellar vesicles. The average size of the aggregates increases with the surfactant concentration, and furthermore, the sizes are slightly larger when the temperature jumps to 35 °C compared to 45 °C. This can be seen in Figure 5 where we show the z-averaged hydrodynamic radius as a function of the surfactant concentration at 35 and 45 °C, respectively.



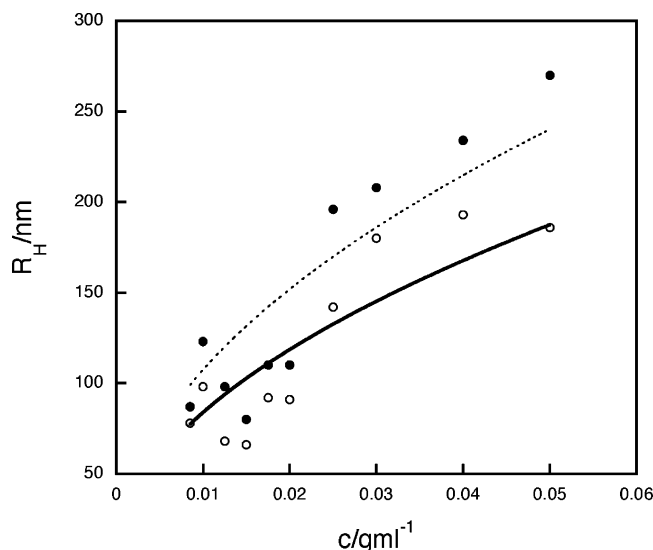


**Figure 5.** Hydrodynamic radius as a function of concentration for temperature jumps from 5 °C to 35 °C (●) and from 5 °C to 45 °C (○). The solid and dotted line is the best fit of data at 35 °C and 45 °C, respectively, to  $\langle R_H \rangle_z = \epsilon \phi^{1/2}$ .

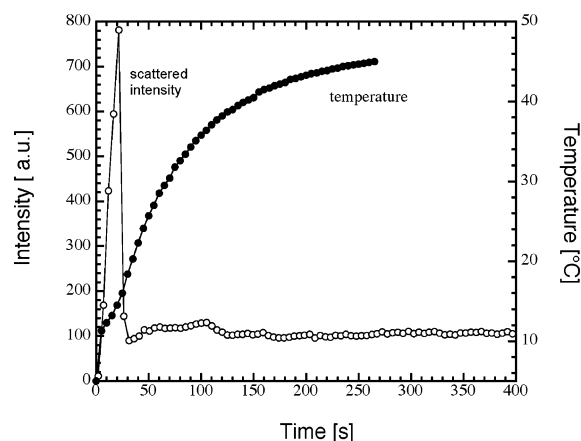


**Figure 6.** Temperature as a function of time for temperature jumps from 5 °C to 45 °C (●). (○) = The scattered light intensity at the angle 90°, measured as the temperature is increased.

This way of changing the temperature, by moving the sample from one bath to another, is rather slow, and the sample spends a considerable time in the temperature range corresponding to the two-phase region  $L_1' + L_1''$ . In Figure 6 we show a temperature–time profile measured by a thermocouple placed in a sample cell filled with pure water, for a 5 to 45 °C temperature change. As can be seen, it takes approximately 30 s until the temperature reaches above the three phase line at 21 °C.

The first major event occurring in the sample as the temperature increases is a phase separation process involving the formation of the concentrated phase  $L_1''$  by the aggregation of micelles. In Figure 6 we also show the variation of the light scattering intensity, measured at the angle 90°, with the time for a sample with the concentration 0.05 wt %.

Also here, the temperature jump was to 45 °C. Initially, the intensity increases rapidly with time, indicating the aggregation of micelles in the two-phase region. However, after approximately 20 s, the intensity reaches a maximum after which it drops rapidly to a value, about 8 times lower than at the maximum, at which then the intensity remains stable. We can understand this nonmonotonic intensity profile as follows. Initially we see the aggregation of micelles into dense particle

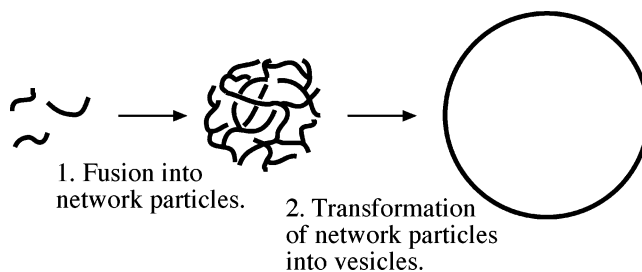


**Figure 7.** A schematic presentation of the transition from wormlike micelles to vesicle via the formation of a network particle.

having approximately the equilibrium structure and composition (30–40 wt % of surfactant) of the  $L_1''$  phase. At very short times the radius of gyration,  $R_g$ , of the particles are relatively small so the scattered intensity at 90° is not much lower than the intensity at zero angle that reports on the average molecular weight of the particles. As the  $R_g$  increases, the intensity increase is slowed compared to that at zero angle, but the intensity still increases as long as the internal structure of the particles remain constant. When the intensity has reached its maximum and now instead decreases with time, the aggregation process has terminated. Instead, there is a local structural reorganization of the particles, at constant number of surfactant molecules, from being dense with a relatively small  $R_g$  to become vesicles with a larger  $R_g$ . At zero angle this process does not lead to an intensity change, but for scattering angles where  $q > 1/R_g$ , the increase in  $R_g$  leads to a significant drop in the scattered intensity. The scenario described above is schematically illustrated in Figure 7.

As the temperature is increased above the phase boundary temperature phase separation begins. Close to the phase boundary we expect a nucleation and growth of the concentrated  $L_1''$  phase. The barrier, which we expect to be very small even close to the phase boundary because of the low interfacial tension between the two aqueous phases, for forming the new phase decreases as one moves deeper into the two-phase region. Above a certain temperature (i.e. the spinodal line) the barrier vanishes and a random aggregation occurs. Assuming that the main events occur above the spinodal line and that fusion events are fast, we can model the formation of large aggregates as diffusion-limited aggregation kinetics.<sup>20,49</sup> For the heteroassociation of two aggregates,  $i$  and  $j$ , we have the rate constant

$$k_{ij} = 4\pi(R_i + R_j)(D_i + D_j) \quad (9)$$

where  $R_i$  and  $R_j$  are collision cross section radii and  $D_i$  and  $D_j$  are their diffusion coefficients, which in dilute solutions are given by the Stokes–Einstein relation and is inversely proportional to the hydrodynamic radius. For small aggregates,  $R_i$  should approximately be given by the radius of gyration, but larger aggregates can be considered as colloidal spheres, and we will use the approximation that all aggregates, irrespective of size, are characterized by a single radius so that

$$k_{ij} = \frac{2k_B T}{3\eta} \left( \frac{1}{R_i} + \frac{1}{R_j} \right) (R_i + R_j) \quad (10)$$

The radius dependence of  $k_{ij}$  is weak and a simplifying approximation is to set  $(R_i^{-1} + R_j^{-1})(R_i + R_j) = 4$  so that the rate constant is size independent and given by

$$k \approx \frac{8k_B T}{3\eta} \quad (11)$$

With this approximation the time dependent size distribution becomes

$$c_n(t) = c^0 \frac{(t/\tau)^{n-1}}{(1 + t/\tau)^{n+1}} \quad (12)$$

where  $n$  is the number of particles in a cluster,  $t$  is the total aggregation time, and  $c^0$  is the initial particle (here, micelle) concentration and

$$\tau = \frac{2}{kc^0} \quad (13)$$

is the characteristic collision time. For  $t \gg \tau$ ,  $c_n$  becomes an exponential function

$$c_n = c^0 e^{-n/\tilde{t}} \quad (14)$$

where we also have defined the relative time  $\tilde{t} = t/\tau$ .

For a total aggregation time,  $t$ , which we expect to correspond approximately to the time spent in the two-phase region  $L_1' + L_1''$ , eq 14 will describe the finally obtained size distribution of vesicles. Equation 14 can be converted into radius distribution function by noting that

$$n = \frac{4\pi R^2 \delta}{v_m} \quad (15)$$

Here,  $R$  is the vesicle radius,  $\delta$  is the bilayer thickness, and  $v_m$  is the micellar volume, which in turn can be written as

$$v_m = n_m v_s \quad (16)$$

where  $n_m$  is the surfactant aggregation number in the initial micelle and  $v_s$  is the volume of a surfactant molecule. For simplicity we neglect the polydispersity of the initial micelles, and  $n_m$  hence corresponds to an average aggregation number. Hence, the aggregation model predicts a Gaussian vesicle radius distribution

$$c(R) = c^0 \exp\{-R^2/2\sigma^2\} \quad (17)$$

with a standard deviation

$$\sigma = \left( \frac{v_{\text{micelle}} t k c_{\text{micelle}}}{4\pi\delta} \right)^{1/2} = \left( \frac{t k \phi}{4\pi\delta} \right)^{1/2} \quad (18)$$

where  $c^0$  still denotes the initial micellar concentration. In principle we expect a cutoff of the distribution function at very small radii. Both because they are strongly punished by curvature energy and because they are unstable relative to flat disks that can fuse and finally form larger vesicles. However, we neglect this additional complication at the present stage and since in the scattering experiments large vesicles have a stronger weight, the exact shape of the distribution curve at small  $R$  is less significant. In the dynamic light scattering experiment, we obtain a  $z$ -averaged or intensity weighted size distribution function,  $c_z(R)$ , where the different vesicle sizes also are weighted according to their scattering power, the radius dependent form factor,  $P(q)$ . Ignoring cross correlations we can write

$$c_z(R, q) = P(R, q) c(R) \quad (19)$$

where the form factor of a vesicle can for  $R \gg \delta$  to a

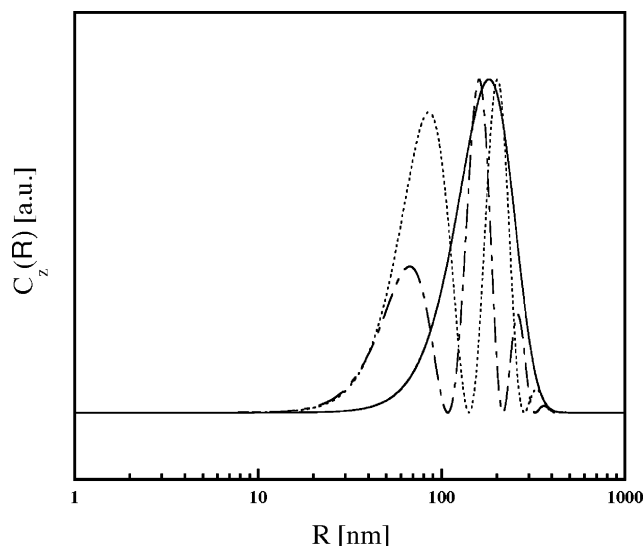


**Figure 8.** Calculated intensity weighted size distribution functions,  $c_z(R)$ , at 45° (solid line), 90° (dotted line), and 135° (dashed line) for  $\sigma = 100$  nm, and  $\lambda_0 = 532$  nm.

good approximation be written as

$$P(R, q) = (4\pi R^2 \delta)^2 \left( \frac{\sin\{qR\}}{qR} \right)^2 \quad (20)$$

For  $q \ll 1/\sigma$ ,  $c_z(R)$  has a single peak at  $R = 2\sigma$ . However, for  $q > 1/\sigma$   $c_z(R)$  will contain several maxima where in between  $c_z(R)$  goes to zero.<sup>50</sup> This is a consequence of a broad size distribution where the trigonometric function of the form factor shows up in the intensity weighted distribution function. In static scattering experiments, the scattering curve  $I(q)$  seldom contains very strong oscillation due to a polydispersity in  $R$ . In real space where  $c_z(R)$  is considered, oscillations can be more visible because of the high resolution in  $q$  when a given scattering angle is selected. In Figure 8 we have plotted calculated  $c_z(R)$  functions at three different scattering angles, 45, 90, and 135°, respectively, for  $\sigma = 100$  nm and  $\lambda_0 = 532$  nm. As can be seen,  $c_z(R)$  has a single peak at 45°, while at higher angles it contains several peaks. The minima occur for  $qR \approx n\pi$ , with  $n$  being an integer  $\geq 1$ . Because the radii of the two first minima only differ by a factor of 2, and the peaks are broad, they are difficult to resolve with the common inverse Laplace transformation method. This issue was not investigated further here.

For a quantitative evaluation of the experimental data we have at present focused on lower angles where a well-defined major peak was observed in the relaxation time distribution function, and from the relaxation time at the peak maximum we have obtained a  $z$ -averaged hydrodynamic radius,  $\langle R_H \rangle_z$ , which was plotted in Figure 5 as a function of  $\phi$  for jumps to 35 and 45 °C, respectively. Identifying  $\langle R_H \rangle_z = 2\sigma$ , as discussed above, we can analyze the variations of  $\langle R_H \rangle_z$  using eq 18. The prediction is a  $\phi^{1/2}$  dependence and shown as solid lines are the best fits of the function  $\langle R_H \rangle_z = \epsilon \phi^{1/2}$  to the two data sets. The values of  $\epsilon$  obtained from the fits are approximately  $10^3$  nm, with a slightly higher value at 35 °C compared to 45 °C. With  $\epsilon$  given by  $\epsilon = (kt/\pi\delta)^{1/2}$  we can calculate  $t$  from the obtained  $\epsilon$  values and compare that to the estimated experimental aggregation times, i.e. the times spent in the two-phase region  $L_1' + L_1''$ .  $k \approx 1.2 \cdot 10^{-17} \text{ m}^3 \text{ s}^{-1}$  at room temperature, and  $\delta \approx 3$  nm. With these values we obtain  $t \approx 0.1$  s, which is approximately 2 orders of magnitude lower than the time spent in the two-phase region during the heating process. This is a significant deviation. However, in the model we have assumed

the aggregation to be diffusion limited. The fact that the experimental aggregation time is longer indicates that only a fraction ( $\approx 1/100$ ) of the collisions are sticky resulting in a fusion event. However, this is not surprising since aggregation processes seldom are purely diffusion controlled. One barrier in the present process could be that the aggregate fusion mainly involves free micellar ends, the concentration of which is limited on the aggregate surfaces.

While we at present only can speculate on possible barriers, we note that the difference in vesicle size obtained for jumps to 35 and 45 °C, respectively, are qualitatively consistent with the model prediction that final vesicle size depends on the time allowed for aggregation in the  $L_1' + L_1''$  region. In preliminary experiments, we have also performed a faster temperature jump by diluting a solution at 5 °C with hot water ( $\approx 85$ ) so that the final temperature was  $\approx 45$  °C. In this procedure the jump time is reduced to around a second, and a vesicle size of approximately 100 nm was obtained.

To understand why vesicles form rather than the equilibrium lamellar phase we need to compare the relative stabilities of vesicles and disks. Below we will discuss the disk and vesicle formation within the framework of curvature free energy. We will assume that vesicles are spherical, and for locally spherical deformations (equal principal curvatures) there is a curvature energy density,  $g_c$ , which, within the harmonic approximation, can be written as

$$g_c = \frac{2\kappa'}{r^2} \quad (21)$$

Here,  $\kappa'$  is the spherical bending rigidity and  $r$  is the radius of curvature. From eq 21 it follows that curvature energy,  $G_c$ , of a vesicle is independent of its radius,  $R_V$ , and is given by

$$G_c = 8\pi\kappa' \quad (22)$$

We recall here that eq 21 is the leading term in an expansion in  $1/r$ . By including the next term in the expansion we should add a term of order  $\kappa_4/R_V^2$  to eq 21 that gives an increasing penalty at small radii.

For a planar disk the curvature and thus the curvature energy are zero. However, they do carry a line energy,  $G_L$ , associated with the unfavorable molecular packing along the rim. With  $l_d$  being the length of the rim,  $G_L$  can be written as

$$G_L = \lambda l_d \quad (23)$$

where  $\lambda$  is the line tension. For a circular disk,  $l_d = 2\pi R_d$ . Based on curvature and line energies, the relative stability of vesicles and disks has been discussed by several authors,<sup>51–53</sup> starting with the pioneering work of Helfrich.<sup>51</sup>

However, before turning to the details of the relative stability of vesicles and disks, we note that experiments indicate<sup>1</sup> that the lamellar phase above the three phase line, coexists at low concentrations with surfactant monomers. In this case, the concentration,  $c_b$ , at the phase boundary of the water rich phase is related to a critical aggregation concentration, similar to the cmc of micelle formation, although it here corresponds to a true phase transition. For small supersaturations we expect a region of metastability for the surfactant monomers, while for higher supersaturations the bilayer aggregates will readily nucleate and grow. Modeling the initial bilayer aggregates as disks there will be a critical disk radius that decreases with increasing concentration or supersaturation in the  $L_1' + L_\alpha$  region. As shown in Appendix A, the critical disk radius,  $R_d^*$ , and the nucleation

barrier height,  $\Delta G_d^*$ , can be written as

$$R_d^* = \frac{\lambda a_s}{4k_B T \ln\{c/c_b\}} \quad (24)$$

and

$$\Delta G_d^* = \frac{\lambda^2 \pi a_s}{8k_B T \ln\{c/c_b\}} \quad (25)$$

respectively, where  $a_s$  is the average interfacial area occupied by a surfactant molecule. For  $C_{12}E_4$ ,  $a_s = 44 \text{ \AA}^2$ .<sup>54</sup>

A simple way to estimate  $\lambda$  is to model the surfactant film at the rims experiencing a locally cylindrical deformation with a cylinder radius of half the bilayer thickness. This is done in Appendix C where we obtain the following estimate of the line tension

$$\lambda = \frac{\pi\kappa_m}{\delta} (1 - \delta H_0)^2 \quad (26)$$

where  $\kappa_m$  is the monolayer bending rigidity. Above the  $L_1' + L_1'' + L_\alpha$  three phase line  $\delta H_0 < 1$ , and  $\lambda$  increases with increasing temperature.  $\kappa_m$  is expected to have the value of a few times the thermal energy  $k_B T$ , and hence the line tension is rather small. To have a significant barrier for the disk nucleation one has to be at very small supersaturations,  $c/c_b < 1.1$ , while we here are working typically at  $c/c_b > 10$ . Hence, we can safely conclude that the aggregate sizes obtained here are much larger than the critical sizes involved in disk nucleation.

The relative stability of disks and vesicles are governed by the dimensionless parameter<sup>53</sup>

$$\alpha = \frac{\lambda A^{1/2}}{4\pi^{1/2}\kappa'} \quad (27)$$

where  $A = \pi R_d^2 = 4\pi R_V^2$  is the bilayer area. For  $\alpha < 1$ , disks are stable relative to vesicles, while the opposite holds for  $\alpha > 1$ . In other words, vesicles are more stable than disks at higher bilayer areas. Due to a barrier in the disc-to-vesicle closing process, vesicle closure is not expected to occur until  $\alpha > 2$ , corresponding to a vesicle radius<sup>51</sup>

$$R_V^* = \frac{4\kappa'}{\lambda} \quad (28)$$

With the estimate for  $\lambda$ , eq 28 can be rewritten as

$$R_V^* = \frac{4\delta}{\pi} \left( \frac{2(1 - \delta H_0/2) + \frac{\bar{\kappa}_m}{\kappa_m}}{(1 - \delta H_0)^2} \right) \quad (29)$$

where we have used eq C1 in (28). Here,  $\kappa_m$  and  $\bar{\kappa}_m$  are the bending and the saddle splay modulus, respectively, of the surfactant monolayer. In particular at 45 °C, we are very close to  $H_0 = 0$ , where eq 29 is simplified to

$$R_V^* = \frac{4\delta}{\pi} \left( 2 + \frac{\bar{\kappa}_m}{\kappa_m} \right) \quad (30)$$

$\kappa_m$  is expected to have a value of a few  $k_B T$ .  $\bar{\kappa}_m$  is for most surfactants less well-known. In general it is expected to be negative and of similar magnitude as  $\kappa_m$ . For the similar surfactant  $C_{12}E_5$ ,  $\kappa_m$  and  $\bar{\kappa}_m$  were recently determined to 2.5 and  $-1 k_B T$ , respectively. In most vesicle systems,  $H_0$  is close

to zero, so eq 30 should apply to a good approximation. We therefore conclude that  $R_V^*$  in general should be very small. If  $\bar{\kappa}_m < 0$ , we typically expect  $R_V^*/\delta < 8/\pi \approx 2.5$ . Experimentally, one generally finds  $R_V^*/\delta$  to be significantly larger, typically of the order of 10. Possibly, the lower limit of vesicle sizes is rather governed by higher order bending rigidities. But the situation is complicated, since, for  $H \gg H_0$  one may have to include higher order curvature terms also in the calculation of the line tension.

For the present C<sub>12</sub>E<sub>4</sub> system,  $\delta \approx 3$  nm. If we have  $R_V^* < 2.5 \delta$ , then  $R_V^* < 7.5$  nm, while the sizes observed experimentally are typically an order of magnitude larger. Hence, we conclude that when the temperature in the T-jump experiment has reached above the three phase line temperature and bilayers are being formed, the aggregate sizes are already much larger than that corresponding to  $R_V^*$  and the aggregates evolve directly into vesicles. We are in a regime where the vesicle sizes are governed by the rate of heating through the two-phase region,  $L_1' + L_1''$  as also demonstrated by the results presented in Figure 5. While there is fast aggregation in the present system, the situation is opposite in to the lecithin-bile salt system studied extensively by Egelhaaf et al.<sup>28,31</sup> There, micellar fusion is slow due to the electrostatic intermicellar repulsion, induced by the charged bile salt.<sup>31</sup>

## 5. Summary

We have studied the formation of vesicles from wormlike micelles, induced by temperature jumps across a liquid–liquid coexistence region. The vesicles are large and polydisperse with an average radius on the order of 200 nm. The vesicle dispersion appears as quasi-stationary. The evolution of the vesicle dispersion toward the formation of a lamellar phase is very slow. The size of the vesicles is affected by how fast the temperature is increased; a slow-temperature jump will give larger vesicles. This is due to the aggregation of the micelles into network particles, which was analyzed in terms of classical colloidal aggregation.

**Acknowledgment.** The authors are grateful to Jörgen Jansson and Håkan Wennerström for fruitful discussions. This work was supported by the Center for Amphiphilic Polymers from renewable Resources (CAP), Stiftelsen för Strategisk Forskning (SSF) within the frame program COLINTECH, the former Swedish Natural Science Research Council (NFR), and the Swedish National Research Council (VR).

## Appendix A

**Disk Nucleation.** To examine the nucleation process we assume that we have surfactant monomers that self-assemble into planar circular bilayer disks. A number,  $n$ , of unimers,  $S$ , form a disk aggregate (of aggregation number  $n$ ),  $S_n$ , according to



The free energy change for this process is

$$\Delta G = n(\mu_n - \mu_1) \quad (\text{A2})$$

where  $\mu_n$  and  $\mu_1$  are the surfactant chemical potentials in a disk of aggregation number  $n$  and in the monomer state, respectively. For the monomer state we have

$$\mu_1 = \mu_1^* + k_B T \ln c_1 \quad (\text{A3})$$

where  $c_1$  is the unimer concentration and  $\mu_1^*$  is the chemical potential in the reference state. To calculate the chemical potential in a disk we assume that the disks are so large (radius much larger than thickness) that the area of the rim is negligible and the aggregation number to a good approximation is given by the relation

$$\pi R_d^2 = \frac{n}{2} a_s \quad (\text{A4})$$

where  $a_s$  is the average area occupied per molecule. For a circular disk, the line energy  $G_L = \lambda 2\pi R_d$  and the free energy of the disk can be written as

$$G_d = n\mu^0 + \lambda(2\pi a_s)^{1/2} n^{1/2} \quad (\text{A5})$$

where we have used eq A4 to relate  $R_d$  to  $n$ .  $\mu^0$  is the chemical potential in the standard state of aggregated molecules, here corresponding to a free planar bilayer. From eq A5 we then obtain the chemical potential

$$\mu_n = \mu^0 + \frac{\lambda a_s}{2R_d} \quad (\text{A6})$$

With eqs A3 and A6 in (A2) we obtain

$$\Delta G = \lambda \pi R_d - \frac{2\pi}{a_s} (\mu_1 - \mu^0) R_d^2 \quad (\text{A7})$$

where aggregate formation occurs when  $\mu_1 > \mu^0$ .

The lamellar phase of the present system is, however, nonswelling, and the equality  $\mu_1 = \mu^0$  does not exactly hold at the phase boundary. In other words, since the lamellar phase that coexists with monomers is concentrated, its chemical potential is also expected to include contributions from interbilayer interactions. Moreover, we expect  $\mu_1^*$  to increase with increasing temperature. Nevertheless, for semiquantitative arguments, we may assume  $\mu_1 = \mu^0$  at the phase boundary, but we will return to this question below.

For  $\mu_1 > \mu^0$ , eq A7 implies the presence of an activation energy for the disk formation. Solving

$$\frac{\partial \Delta G}{\partial R_d} = 0 \quad (\text{A8})$$

we obtain the activation energy

$$\Delta G_d^* = \frac{\lambda^2 \pi a_s}{8(\mu_1 - \mu^0)} \quad (\text{A9})$$

and the critical disk radius

$$R_d^* = \frac{\lambda a_s}{4(\mu_1 - \mu^0)} \quad (\text{A10})$$

with

$$\frac{\Delta G_d^*}{R_d^*} = \frac{\lambda \pi}{2} \quad (\text{A11})$$

Defining the phase boundary concentration as  $c_b$  and assuming  $\mu^0 = \mu_1 = \mu^* + k_B T \ln c_b$  at the phase boundary



of the given temperature we have

$$\Delta G_d^* = \frac{\lambda^2 \pi a_s}{8k_B T \ln\{c/c_b\}} \quad (\text{A12})$$

and

$$R_d^* = \frac{\lambda a_s}{4k_B T \ln\{c/c_b\}} \quad (\text{A13})$$

where  $c/c_b$  is the relative supersaturation. As mentioned above, we expect  $\mu^0$  to be slightly lower than  $\mu^* + k_B T \ln c_b$  and hence eqs A12 and A13 to overestimate the activation energy and the critical radius.

## Appendix B

**Relative Stability of Disks and Vesicles and Vesicle Closure.** Within the harmonic approximation (eqs 21 and 22), the vesicle curvature energy is radius independent, while the line energy increases with the square root of the bilayer area for a circular disk (eq 23). Hence we expect vesicles to be favored relative to disks at higher bilayer areas. The free energy difference between vesicle and disk can be expressed as

$$\frac{\Delta G}{\kappa'} = 8\pi(1 - \alpha) \quad (\text{B1})$$

where  $\alpha$  is the dimensionless stability parameter given by

$$\alpha = \frac{\lambda A^{1/2}}{4\pi^{1/2} \kappa'} \quad (\text{B2})$$

Here,  $A = \pi R_d^2 = 4\pi R_V^2$  is the bilayer area. For  $\alpha < 1$ , disks are stable relative to vesicles while the opposite holds for  $\alpha > 1$ . When a bilayer fragment or disk closes into a vesicle, the length of the unfavorable rim decreases and finally vanishes when the vesicle is formed. At the end of this process one essentially has a vesicle with a hole, where the hole finally closes. As the limit of a flat bilayer we consider a circular disk of area  $A$ . In the closing process we assume that the bilayer is bent spherically, as illustrated in Figure 9, meaning that the two principal curvatures are equal everywhere.

During the closing process the radius of curvature,  $r$ , will decrease from infinity for the flat disk, finally approaching  $R_V$ , the vesicle radius, with  $A = 4\pi R_V^2$ . Restricting ourselves to

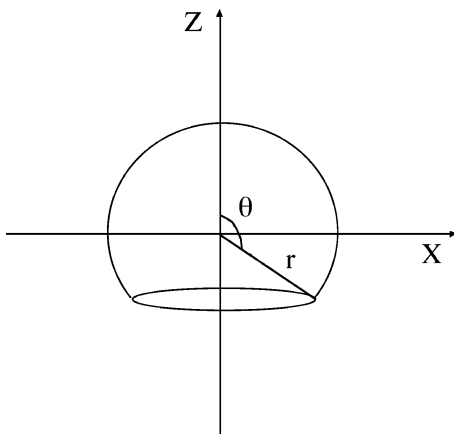


**Figure 9.** Vesicle closure. The bilayer is bent spherically with azimuthal angle  $\theta$ , which increase from 0 for flat disks to  $\pi$  for closed vesicles. Radius of curvature  $r$  can reach values from infinity for flat bilayer to  $R_V$ , vesicle radius, when the vesicle is closed.

spherical bending, the intermediate bilayer structure can be described in terms of the solid angle,  $\Omega$ , where  $\Omega = 0$  for the disk and  $\Omega = 4\pi$  for vesicle. The bilayer area is then given by  $A = \Omega r^2$ , with  $r$  being the radius of curvature. It is convenient to express the solid angle in terms of the azimuthal angle,  $\theta$  (see Figure 9), i.e.  $\Omega = 2\pi(1 - \cos\theta)$  and  $0 \leq \theta \leq \pi$ . At a given  $\theta$  (or  $\Omega$ ), the curvature energy is given by

$$G_C = 2\kappa'\Omega = 4\pi\kappa'(1 - \cos\theta) \quad (\text{B3})$$

and the line energy can be written as

$$G_L = 2\pi\lambda r \sin\theta = (2\pi A(1 + \cos\theta))^{1/2}\lambda \quad (\text{B4})$$

The total energy,  $G = G_C + G_L$ , can finally be expressed in terms of the dimensionless parameter  $\alpha$  and the angle  $\theta$ , and we can write

$$G/\kappa' = 4\pi[(1 - \cos\theta) + \alpha(2(1 + \cos\theta))^{1/2}] \quad (\text{B5})$$

Eq B5 describes the energy variation as a disk is bent spherically to finally form a closed vesicle. The intermediate bilayer shape is described by the angle  $\theta$ , and the parameter  $\alpha$  controls the relative stability of a disk and a vesicle. Note that it also can describe the reverse process, i.e. the transformation of vesicle to a disk. The assumptions involved are that the total energy is simply the sum of a curvature and a line energy where the line tension  $\lambda$  does not vary with the geometry of the line, for example the radius of a circular hole. Hence, we neglect for example any possible barrier in the initial nucleation of a hole in a vesicle in a vesicle-to-disk transformation.

When  $\alpha$  is only weakly larger than unity, there may still be a significant barrier for process of closing the bilayer into a vesicle.  $G$  has a maximum at the angle  $\theta^*$  where

$$\cos\theta^* = \frac{\alpha^2}{2} - 1 \quad (\text{B7})$$

and the activation energy,  $\Delta G^* = G(\theta^*) - G_d$ , for the vesicle closure is

$$\Delta G^* = 8\pi\kappa'\left(1 - \frac{\alpha^2}{2}\right)^2 \quad (\text{B8})$$

The barrier in the opposite direction, i.e. the vesicle-to-disk transition, is in a similar way given by  $\Delta G^* = G(\theta^*) - G_V = 2\pi\kappa'\alpha^2$ .

Since  $\kappa'$  in general has the value of a few times  $k_B T$ , the disc-to-vesicle transition will occur at  $\alpha$ -values close to 2 rather than when  $\alpha = 1$ . For simplicity we can define  $\alpha = 2$  as the transition point, i.e., where  $\Delta G^*$  vanishes. The vesicle radius corresponding to this  $\alpha$ -value is

$$R_V = \frac{4\kappa'}{\lambda} \quad (\text{B9})$$

and is hence the vesicle radius expected when vesicles are from from the closure of growing disks. This result was also obtained by Helfrich<sup>51</sup> although derived in a slightly different way.

## Appendix C

**Modeling the Line Tension.** The origin of the line tension is the large deviation of the curvature at the edge from the spontaneous curvature of the surfactant monolayer. A simple model for the line energy is to model the edge as a monolayer bent cylindrically with a cylindrical radius of  $\delta/2$ , where  $\delta$  is

the bilayer thickness (twice the monolayer thickness). For a cylindrical shape the Gaussian curvature is zero and the curvature energy density can be written as

$$g_c = 2\kappa_m \left( \frac{1}{\delta} - H_0 \right)^2 \quad (\text{C1})$$

Here,  $\kappa_m$  is the monolayer bending rigidity and  $H_0$  is the monolayer spontaneous curvature. Hence, modeling the edge as a hemicylinder we find the energy

$$G_{\text{edge}} = \frac{\pi\kappa_m}{\delta} (1 - \delta H_0)^2 l_{\text{edge}} \quad (\text{C2})$$

where  $l_{\text{edge}}$  is the total length of the edge, and hence the line tension is given by

$$\lambda = \frac{\pi\kappa_m}{\delta} (1 - \delta H_0)^2 \quad (\text{C3})$$

According to eq C3 the line tension depends on the spontaneous curvature and has a minimum of zero when  $H_0 = 1/\delta$ . For nonionic, oligo ethylene oxide based surfactants it is well-known that  $H_0$  decreases with increasing temperature. When the bilayer is modeled as two parallel monolayer surfaces at distance  $\delta$  apart, the relations between the bilayer and monolayer elastic moduli are given by

$$\kappa = 2\kappa_m \quad (\text{C4})$$

$$\bar{\kappa} = 2\bar{\kappa}_m - 2\kappa_m \delta H_0 \quad (\text{C5})$$

Since  $\kappa' = \kappa + \bar{\kappa}/2$  we have

$$\kappa' = 2\kappa_m (1 - \delta H_0/2) + \bar{\kappa}_m \quad (\text{C6})$$

and hence

$$\frac{\lambda}{\kappa'} = \frac{\pi(1 - \delta H_0)^2/\delta}{2(1 - \delta H_0/2) + \frac{\bar{\kappa}_m}{\kappa_m}} \quad (\text{C7})$$

As mentioned above,  $\lambda = \lambda/\kappa' = 0$  when  $H_0 = 1/\delta$ . When  $H_0 = 0$ , corresponding to the maximum stability of the planar bilayer, we have

$$\frac{\lambda}{\kappa'} = \frac{\pi\kappa_m}{\delta(2\kappa_m + \bar{\kappa}_m)} \quad (\text{C8})$$

## References and Notes

- (1) Strey, R. *Ber. Bunsen-Ges. Phys. Chem.* **1996**, 100, 182.
- (2) Shinoda, K.; Nakagawa, T.; Tamamushi, B.; Isemura, T. *Colloidal Surfactants*; Academic Press: New York, 1963.
- (3) Schick, M. J. *Nonionic Surfactants*; Marcel Decker Inc.: New York, 1967; Vol. 1.
- (4) Mitchell, D. J.; Tiddy, G. J. T.; Waring, L.; Bostock, T.; McDonald, M. P. *J. Chem. Soc., Faraday* **1983**, 79, 975.
- (5) Shinoda, K. *Prog. Colloid Polym. Sci.* **1983**, 68, 1.
- (6) Fendler, J. *Membrane Mimetic Chemistry*; Wiley: New York, 1983.
- (7) *Liposomes: From Biophysics to Therapeutics*; Dekker: New York, 1987.
- (8) Olsson, U.; Nakamura, K.; Kunieda, H.; Strey, R. *Langmuir* **1996**, 12, 3045.
- (9) Kunieda, H.; Nakamura, K.; Davis, H. T.; Evans, D. F. *Langmuir* **1991**, 7, 1915.
- (10) Kunieda, H.; Nakamura, K.; Evans, D. F. *J. Am. Chem. Soc.* **1991**, 113, 1051.
- (11) Strey, R. *Colloid Polym. Sci.* **1994**, 272, 1005.
- (12) Olsson, U.; Wennerström, H. *Adv. Colloid Interface Sci.* **1994**, 49, 113.
- (13) Cates, M. E.; Candau, S. J. *J. Phys.: Condens. Matter* **1990**, 2, 6869.
- (14) Ambrosone, L.; Angelico, R.; Ceglie, A.; Olsson, U.; Palazzo, G. *Langmuir* **2001**, 17, 6822.
- (15) Drye, T. J.; Cates, M. E. *J. Chem. Phys.* **1996**, 2, 1367.
- (16) Anderson, D.; Wennerström, H.; Olsson, U. *J. Phys. Chem.* **1989**, 89, 4243.
- (17) Bangham, A. D.; Horne, R. W. *J. Mol. Biol.* **1964**, 8, 660.
- (18) Israelachvili, J. *Intermolecular and surface forces*, 2nd ed.; Academic Press: 1991.
- (19) Lasic, D. D. *Liposomes*; Elsevier: Amsterdam, 1993.
- (20) Evans, D. F.; Wennerström, H. *The Colloidal Domain where Physics, Chemistry, Biology and Technology meet*; 2nd ed.; Wiley-VHC: New York, 1998.
- (21) Kaler, E. W.; Murthy, A. K.; Rodriguez, B. E.; Zasadzinski, J. A. N. *Science* **1989**, 245, 1371.
- (22) Marques, E.; Khan, A.; Miguel, M. d. G.; Lindman, B. *J. Phys. Chem.* **1993**, 97, 4729.
- (23) Joannic, R.; Auvray, L.; Lasic, D. D. *Phys. Rev. Lett.* **1997**, 78, 3402.
- (24) Schleifer, I.; Gerasimov, O. V.; Thompson, D. H. *Proc. Natl. Acad. Sci. U.S.A.* **1998**, 95, 1032.
- (25) Khan, A.; Marques, E. F. *Curr. Opin. Colloid Interface Sci.* **2000**, 4, 402.
- (26) Olsson, U.; Wennerström, H. *J. Phys. Chem.* **2002**, 106, 5135.
- (27) Gradzielski, M. *Curr. Opin. Colloid Interface Sci.* **2003**, 8, 337.
- (28) Egelhaaf, S. U.; Schurtenberger, P. *Phys. Rev. Lett.* **1999**, 82, 2804.
- (29) Egelhaaf, S. U.; Olsson, U.; Schurtenberger, P. *Physica B (Amsterdam)* **2000**, 276–278, 326.
- (30) Leng, J.; Egelhaaf, S. U.; Cates, M. E. *Europhys. Lett.* **2002**, 59, 311.
- (31) Leng, J.; Egelhaaf, S. U.; Cates, M. E. *Biophys. J.* **2003**, 85, 1624.
- (32) Schillén, K.; Bryskhe, K.; Melnikova, Y. S. *Macromolecules* **1999**, 32, 6885.
- (33) Bryskhe, K.; Jansson, J.; Topgaard, D.; Schillén, K.; Olsson, U. *J. Phys. Chem. B* **2004**, 108, 9710.
- (34) Lee, T. D.; Olsson, U.; Wennerström, H.; Schurtenberger, P. *Phys. Rev. E* **1999**, 60, 4300.
- (35) Jansson, J.; Schillén, K.; Olofsson, G.; da Silva, R. C. **2003**, in press.
- (36) Schurtenberger, P.; Newman, M. E. In *Environmental Particles*; Buffle, J.; Leeuwen, H. P. v., Eds.; Lewis Publisher: Boca Raton, 1993.
- (37) Schurtenberger, P.; Augusteyn, R. C. *Biopolymers* **1991**, 31, 1229.
- (38) Henriksson, U.; Jonströmer, M.; Olsson, U.; Söderman, O.; Klose, G. *J. Phys. Chem. B* **1991**, 95, 3815.
- (39) Schurtenberger, P.; Cavaco, C. *J. Phys. II Fr.* **1993**, 3, 1279.
- (40) Schurtenberger, P.; Cavaco, C. *Langmuir* **1994**, 10, 100.
- (41) Schurtenberger, P.; Cavaco, C. *J. Phys. Chem.* **1994**, 98, 5481.
- (42) Schurtenberger, P.; Cavaco, C. *Langmuir* **1996**, 12, 2894.
- (43) Richtering, W. H.; Burchard, W.; Jhans, E.; Finkelmann, H. *J. Phys. Chem. B* **1988**, 92, 6032.
- (44) Otha, T.; Oono, Y. *Phys. Lett.* **1982**, 89A, 460.
- (45) Wiltzius, P.; Haller, H.; Cannell, D. S. *Phys. Rev. Lett.* **1983**, 51, 1183.
- (46) Brown, W.; Nicolai, T. *Colloid Polym. Sci.* **1990**, 268, 977.
- (47) Bulut, S. Diploma Thesis, University of Lund, 2002.
- (48) Glatter, O.; Kratky, O. *Small Angle X-ray Scattering*; Academic Press: London, 1982.
- (49) Kruyt, H. R. *Colloidal Sci.* Elsevier: New York, 1952; Vol. 1.
- (50) Pusey, P. N.; Megan, W. v. *J. Chem. Phys.* **1984**, 80, 3513.
- (51) Helfrich, W. *Phys. Lett.* **1974**, 50A, 115.
- (52) Lasic, D. D. *Biochim. Biophys. Acta* **1982**, 692, 501.
- (53) Fromherz, P. *Chem. Phys. Lett.* **1983**, 94, 259.
- (54) Le, T. D.; Olsson, U.; Mortensen, K. *Phys. Chem. Chem. Phys.* **2001**, 3, 1310.